

Available at www.sciencedirect.com

ScienceDirect

journal homepage: www.elsevier.com/locate/modo

SRF is essential for mesodermal cell migration during elongation of the embryonic body axis

Benedikt Schwartz ^{a,b}, Matthias Marks ^a, Lars Wittler ^a, Martin Werber ^a, Sandra Währisch ^a, Alfred Nordheim ^c, Bernhard G. Herrmann ^a, Phillip Grote ^{a,*}

^a Max Planck Institute for Molecular Genetics, Department of Developmental Genetics, Ihnestr. 63-73, 14195 Berlin, Germany

^b Free University Berlin, Dept. of Biology, Chemistry and Pharmacy, Takustr. 3, 14195 Berlin, Germany

^c Department of Molecular Biology, Interfaculty Institute for Cell Biology, University of Tübingen, 72076 Tübingen, Germany

ARTICLE INFO

Article history:

Received 24 September 2013

Received in revised form

1 July 2014

Accepted 3 July 2014

Available online 11 July 2014

Keywords:

Serum Response Factor (SRF)

Brachyury

Mouse embryo

Body axis elongation

Migration

Epithelial–mesenchymal transition

ABSTRACT

Mesoderm formation in the mouse embryo initiates around E6.5 at the primitive streak and continues until the end of axis extension at E12.5. It requires the process of epithelial-to-mesenchymal transition (EMT), wherein cells detach from the epithelium, adopt mesenchymal cell morphology, and gain competence to migrate. It was shown previously that, prior to mesoderm formation, the transcription factor SRF (Serum Response Factor) is essential for the formation of the primitive streak. To elucidate the role of murine *Srf* in mesoderm formation during axis extension we conditionally inactivated *Srf* in nascent mesoderm using the *T(s)::Cre* driver mouse. Defects in mutant embryos became apparent at E8.75 in the heart and in the allantois. From E9.0 onwards body axis elongation was arrested. Using genome-wide expression analysis, combined with SRF occupancy data from ChIP-seq analysis, we identified a set of direct SRF target genes acting in posterior nascent mesoderm which are enriched for transcripts associated with migratory function. We further show that cell migration is impaired in *Srf* mutant embryos. Thus, the primary role for SRF in the nascent mesoderm during elongation of the embryonic body axis is the activation of a migratory program, which is a prerequisite for axis extension.

© 2014 Elsevier Ireland Ltd. All rights reserved.

1. Introduction

During vertebrate development the embryonic body grows in an anterior to posterior direction. Elongation of the antero-posterior (A–P) axis depends on the progressive addition of new tissue at the posterior end of the embryo, which is generated by a transient structure called the primitive streak (ps). In mouse embryos, the ps forms at embryonic day (E) 6.5 and is replaced by the tail bud at mid-somite stages (E9.25–E9.5, ≥ 22 somites) (for review, see [Beddington, 1983](#)).

Cells located in the ps differentiate into mesendodermal tissue, marked by the expression of genes such as *Brachyury* (*T*) ([Herrmann, 1991](#)). These cells undergo an epithelial-to-mesenchymal transition (EMT), allowing them to become motile, migrate away from the ps, and intercalate between the definitive endoderm and ectoderm (reviewed in [Baum et al., 2008](#)). Epithelial epiblast cells provide a constant source of mesodermal cells. At E7.5 a complete layer of mesoderm has formed between the ectoderm and endoderm, but EMT continues until axis elongation ceases between E12.5 and E13.5 ([Cunningham et al., 2011](#)).

* Corresponding author.

E-mail address: grote@molgen.mpg.de (P. Grote).

<http://dx.doi.org/10.1016/j.mod.2014.07.001>

0925-4773/© 2014 Elsevier Ireland Ltd. All rights reserved.

EMT has been shown to be a central process during various stages of embryonic development including gastrulation, neural crest formation, and heart morphogenesis (Lim and Thiery, 2012). Moreover, the essential role of EMT in tumor metastasis has been well studied. EMT is a multistep process that comprises the degradation of cell–cell contact proteins (e.g., E-cadherin), the breakdown of the basement membrane, and the regulation of cytoskeletal reorganization (Nakaya and Sheng, 2008; Levayer and Lecuit, 2008). As a consequence, mesenchymal cells lose contact with their neighboring cells, which is a prerequisite for migratory capacity, and they adopt a more extended and elongated shape.

The molecular basis that underlies EMT during mouse gastrulation is only partly understood. Genetic studies in mice have demonstrated that FGF induces downregulation of E-cadherin in ps cells, both at the transcriptional and post-transcriptional levels (Ciruna and Rossant, 2001; Zohn et al., 2006), thereby inducing the delamination of cells from the epithelium. In addition to FGF, several other extracellular signaling molecules contribute to EMT in generating mesodermal cells, including members of the Wnt and TGF β families (Ben-Haim et al., 2006; Kemler et al., 2004). It has also been shown that Wnt signaling is required to specify a pool of multipotent stem cells in the caudal region of vertebrate embryos (Martin and Kimelman, 2012), and that these axial stem cells are required for vertebrate axis extension (for review see Wilson et al., 2009). The molecular characterization of these stem cells is pending, but it is already established that Sox genes are involved in their function (Yoshida et al., 2014).

The gene encoding the transcription factor Serum Response Factor (SRF) is expressed in the ps and newly formed mesoderm in several vertebrates at early stages of gastrulation (Barron et al., 2005; Croissant et al., 1996; Mohun et al., 1991), but its role during mesoderm development and axis elongation has not received careful investigation. SRF is a homodimeric MADS-box-containing transcription factor, which binds a 10 bp sequence known as the CA β G box (Norman et al., 1988; Shore and Sharrocks, 1995). More than 170 *bona fide* SRF target genes have been identified (reviewed in Miano, 2008). These mainly comprise genes involved in muscle cell differentiation, as well as the regulation of cell growth, cell survival, and cell motility (Johansen and Prywes, 1995; Miano, 2003).

Srf^{-/-} mouse embryos show severe gastrulation defects, including lack of the ps, and die at mid-gestation (Arsenian et al., 1998). *Srf* mutants lack all mesodermal tissue and begin to be resorbed from stage E8.5 onwards. While these data identified SRF as a regulator of mesoderm induction, they did not provide insight into the role that SRF plays once the ps has formed. Thus, in order to study the role of SRF during axis elongation, we conditionally deleted *Srf* in murine ps cells using Cre recombinase driven by the *Brachyury* (*T*) promoter region responsible for *T* expression in the ps (*T(s)::Cre*) (Feller et al., 2008). The resulting mutant embryos displayed, amongst other defects, severe axis truncation – indicating that SRF is essential for axis elongation. We present both molecular and functional data to demonstrate that SRF is required for mesodermal cell migration during axis elongation. This identifies SRF as a main player in the EMT process

during gastrulation and the subsequent mesodermal cell movements that are essential for axis elongation.

2. Results

2.1. Conditional deletion of *Srf* in *Brachyury*-expressing cells causes an arrest of axis elongation

In order to investigate the role of SRF during trunk development, we first analyzed its expression pattern in mid-gestational embryos. Whole mount *in situ* hybridization of E9.5 mouse embryos showed domains of increased *Srf* expression in the forebrain, the branchial arches, the intermediate mesoderm and in the paraxial mesoderm and caudal end (Fig. 1A). Expression of *Srf* in nascent mesodermal tissue (such as the paraxial mesoderm) suggested a possible role in mesoderm development during axis elongation. To analyze the function of SRF in nascent mesoderm we generated mouse embryos lacking *Srf* in that tissue using the Cre/loxP system. *Brachyury* (*T*) is one of the earliest markers of mesoderm during development (Herrmann, 1991), thus, we crossed the *Srf*^{flex1/flex1} mouse line carrying a loxP flanked exon one of *Srf* (Wiebel et al., 2002) with the *T(s)::Cre* (C57Bl/6J^{Tg(T-cre)1Gos}) line expressing Cre recombinase under control of the *T_{streak}* promoter of *T*, comprised of the 600 bp upstream of the ATG codon (Feller et al., 2008). This results in a reduction of *Srf* in anterior mesoderm of E8.5 embryos and a complete loss *Srf* expression in posterior mesodermal tissue (Fig. 2B).

The morphology of *Srf*^{flex1/flex1}; *T(s)::Cre* embryos was indistinguishable from wild type embryos until E8.5, but at E8.75 embryos showed malformations of the heart, the allantois, and had an overall smaller appearance (Fig. 1C and D). At E9.5, axis elongation in the mutants had been fully arrested, demonstrating an essential function for SRF in this process. At E10.5 no viable *Srf*^{flex1/flex1}; *T(s)::Cre* embryos were observed. The role of SRF in heart development has already been described (Parlakian et al., 2004), and abnormalities of the heart and allantois, resulting in defective nutrient and gas exchange, are the likely cause of death in the current model. In addition, this phenotype is in full agreement with previously observed impairment of mesoderm formation upon constitutive *Srf* deletion (Arsenian et al., 1998).

2.2. Mesenchymal character is not impaired in cells of the *Srf*^{flex1/flex1}; *T(s)::Cre* embryo caudal end

The arrest of axis elongation observed here could be caused by the loss of mesoderm cells, therefore differing from *Wnt3a* or *Brachyury* mutant embryos where mesoderm induction and formation is impaired (Takada et al., 1994; Wilkinson et al., 1990). In order to investigate this possibility we tested for the presence of BRACHYURY-positive cells in *Srf* mutant embryos by immunohistochemistry. *Srf* mutants have a significant number of BRACHYURY positive cells, indicating that mesoderm is indeed formed upon loss of SRF in cells progressing through the ps (Fig. 2A). An early hallmark of mesoderm formation is the initiation of EMT in the ps accompanied by loss of the cell surface marker E-cadherin. In *Srf* mutants EMT seems to be initiated, as E-cadherin is present

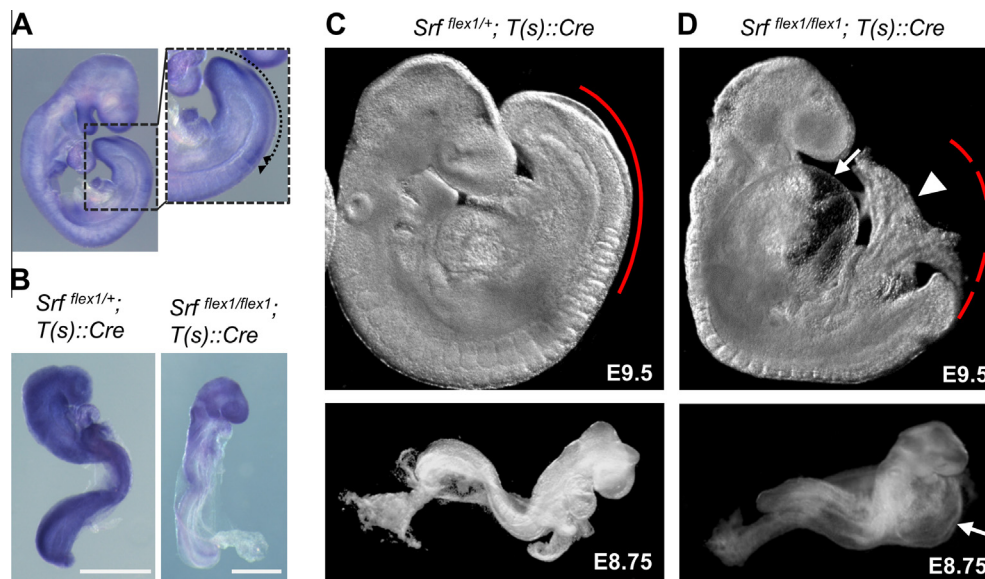


Fig. 1 – Brachyury(T)-driven loss of SRF results in arrest of axis elongation. (A) Whole mount in situ hybridization of *Srf* in a wild type mouse embryo at E9.5. *Srf* transcript is widespread, but strong expression can be observed in the fronto-nasal process, the maxillo-mandibular cleft and first branchial arch, the intermediate mesoderm, and the paraxial mesoderm in the caudal region of the embryo (indicated by the dashed line) up to the forming somitomeres (indicated by arrowheads). **(B)** *Srf* transcript is reduced in *Srf*^{flex1/flex1}; *T(s)::Cre* Embryos in all mesodermal derived tissues and not detectable in the posterior mesodermal tissues even after prolonged staining. Scale bar = 500 μ m. **(C)** *Srf*^{flex1/+}; *T(s)::Cre* embryos at E8.75 and E9.5 exhibit a normally extended antero-posterior axis (indicated by red line). **(D)** *Srf*^{flex1/flex1}; *T(s)::Cre* embryos (E8.75 and E9.5) display malformations in the heart (arrow) and the allantois (arrowhead). At E8.75, they have a normally extended antero-posterior axis, while at E9.5, they display axis truncation (indicated by the dashed line), among other developmental defects.

in the epithelium surrounding the mesoderm, but not in the mesodermal cells of the caudal end (Fig. 2A). In addition, the mesenchymal marker Vimentin could be detected in the early mesoderm (Fig. 2A), further demonstrating that these cell have undergone EMT.

SRF was previously shown to promote cell survival in embryos by inhibiting apoptosis (Schratt et al., 2004). We quantitatively assessed the number of apoptotic cells by counting Annexin V positive cells that were not necrotic (PI positive) in heads and caudal ends from single SRF mutants or control embryos by flow cytometry. In heads and caudal ends from E8.75 (TS13/14) control embryos we could detect $10.4\% \pm 1.8\%$ and $10.5\% \pm 1.7\%$ apoptotic cells, respectively (Fig. 2C and D). In SRF mutants the number of apoptotic cells in heads and caudal ends increased to $34.5\% \pm 1.0\%$ and $23.7\% \pm 1.5\%$, respectively (Fig. 2C and D). We also measured the number of mitotic cells by staining for histone 3 serine 10 phosphorylation (H3S10P) and were not able to detect any changes (Fig. 2E and F). The increase in the number of apoptotic cells might explain the overall smaller appearance of the SRF mutant embryos, but is not sufficient to explain the axis truncation defect.

2.3. RNA expression and ChIP data identified 25 direct SRF target genes during axis elongation

To elucidate the molecular mechanism behind the observed axis truncation phenotype, we dissected posterior ends composed of late ps and unsegmented, nascent meso-

derm from *Srf*^{flex1/flex1}; *T(s)::Cre* embryos and their heterozygous littermates. We examined gene expression at three distinct stages: (i) before malformations in the mutants became apparent (E8.5; 3–9 somites), (ii) when heart and allantoic malformations were visible, but before axis truncation was apparent (E8.75; 11–13 somites), and (iii) when axis elongation arrested (E9.0; 14–16 somites). As expected, *Srf* was downregulated at all three stages (Fig. 3), demonstrating that *Srf* is effectively inactivated in caudal mesoderm by *T(s)::Cre* activity. Coincident with the observed increasing severity of the mutant phenotype, the total number of dysregulated genes increased from 10 genes at E8.5 to 139 genes at E8.75 and 439 genes at E9.0 (fold change $\geq \log 2^{0.4}$, $p < 0.05$; $n = 4$) (Table 1).

To distinguish between direct and indirect targets of SRF during the process of axis extension, we used a genome-wide approach to search for genomic regions bound by SRF, via chromatin immunoprecipitation (ChIP). Chromatin was derived from P19 mouse embryonal carcinoma cells engineered to stably overexpress *Srf*. P19 cells are pluripotent and thus able to differentiate into derivatives of all three germ layers (McBurney, 1993). They are reminiscent of epiblast cells from the early post-implantation blastocyst, and are often used to study events occurring during gastrulation (van der Heyden and Defize, 2003; Yeom et al., 1996).

ChIP-seq analysis identified SRF-bound genomic regions throughout the genome. Previous work demonstrated that the vast majority of SRF binding sites reside within 4000 bp from the transcriptional start site (TSS) of a regulated gene

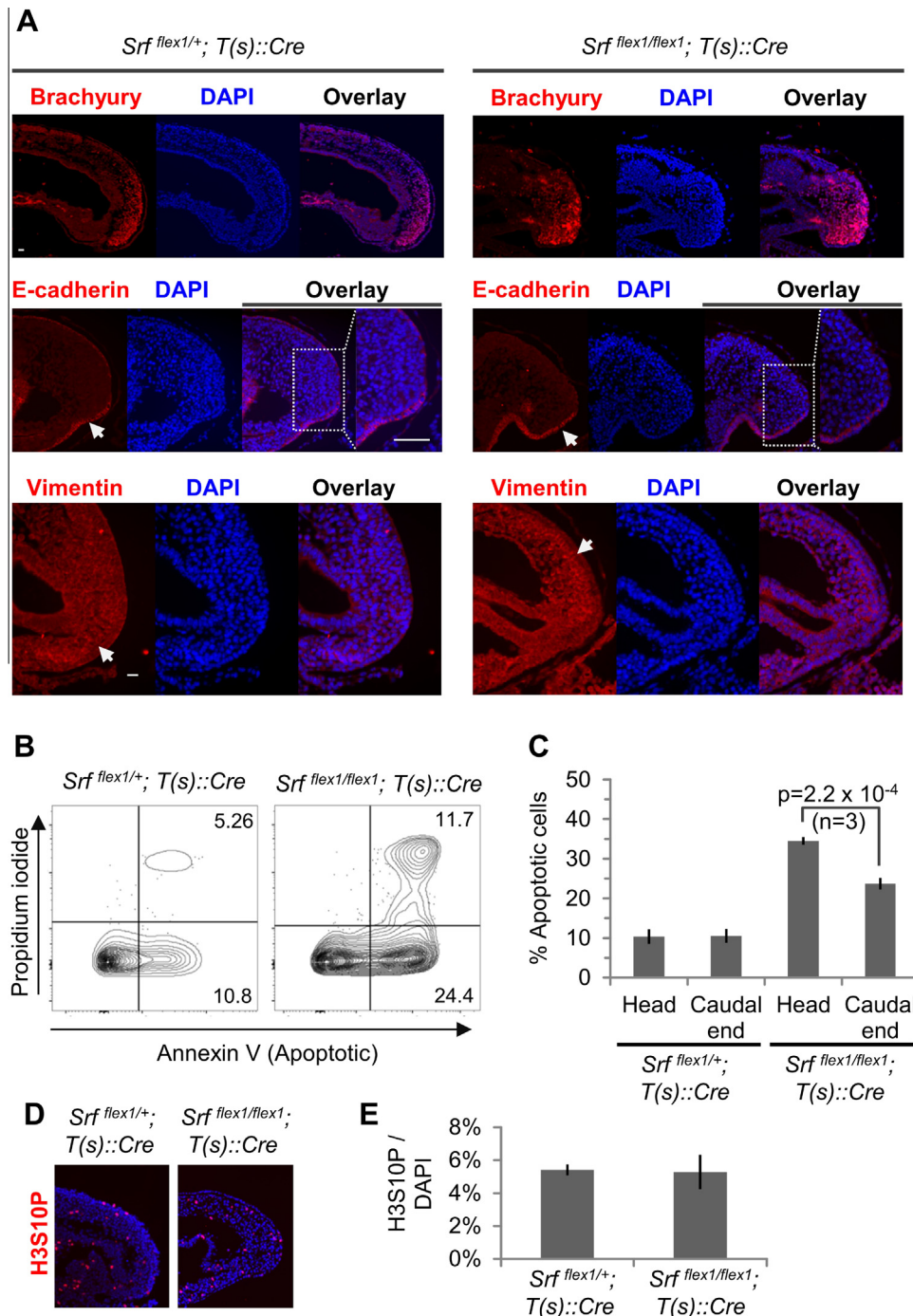


Fig. 2 – Mesoderm formation in *Srf^{flex1/flex1}; T(s)::Cre* embryos. Immunohistological analysis on sagittal sections of caudal ends from E9.0 *Srf^{flex1/flex1}; T(s)::Cre* and control *Srf^{flex1/+}; T(s)::Cre* littermates. (A) Nascent mesoderm and epithelial cells were immunostained for BRACHYURY, E-cadherin and Vimentin. Sections were counterstained with DAPI to visualize nuclei. Arrows indicate the epithelial E-cadherin signal and the mesenchymal Vimentin signal, respectively. The scale bar represents 50 μm . (B) Representative flow cytometry analysis of Annexin V (apoptotic) and PI positive (necrotic) cells from single caudal ends isolated from early E9.0 embryos. The two contour scatterplots depict 3117 (left) and 3066 (right) single cell events and the percentages of cells that fall into the given gate. (C) Quantification of apoptotic cells ($n = 3$) from heads and caudal ends of single embryos. The standard deviation (s.d.) is given. (D) Representative immunostaining of H3S10P indicates mitotic cells in sagittal sections of caudal region of embryos at E9.0. (E) Quantification of the number of mitotic (H3S10P) to the number of total cells (DAPI) in presomitic mesoderm from three consecutive sections from two different embryos. The s.d. is given.

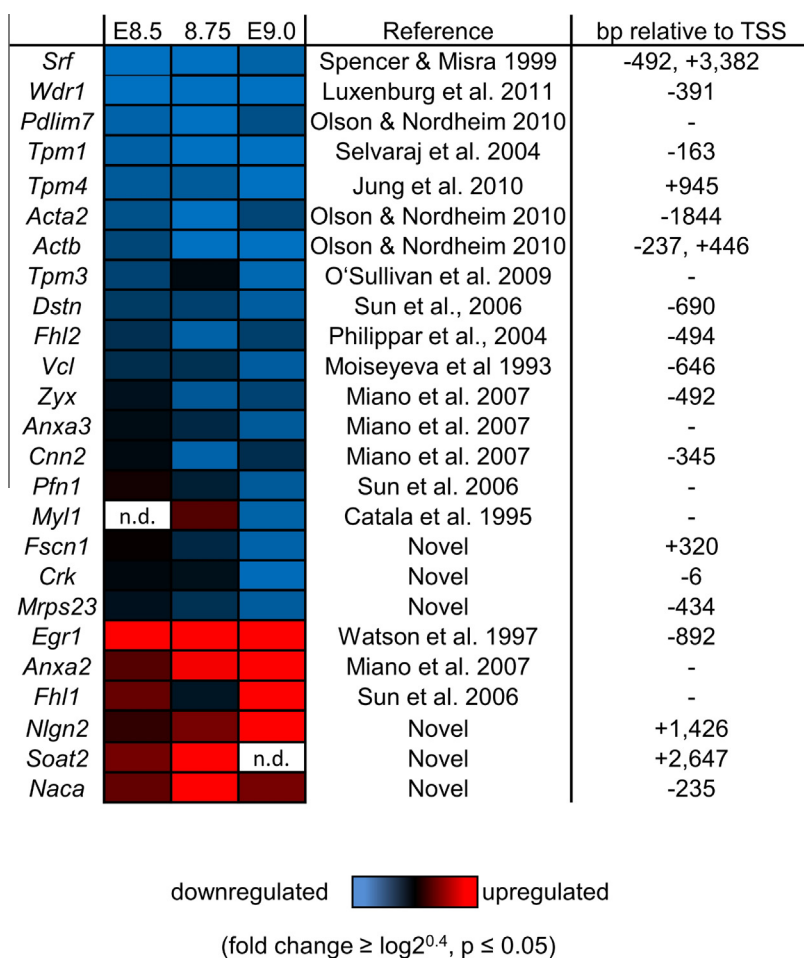


Fig. 3 – Direct target genes of SRF during axial elongation. Identification of direct SRF target genes which are dysregulated in caudal ends of *Srf^{flex1/flex1}; T(s)::Cre* embryos. The heat map indicates the degree of dysregulation at E8.5, E8.75 and E9.0. References are given for genes that have been previously identified as SRF targets. The position of SRF enrichment peaks identified in P19 cells is indicated with respect to the transcriptional start site (TSS). [n.d. = not detectable.] (See above-mentioned references for further information.)

Table 1 – Number of significantly dysregulated genes in *Srf^{flex1/flex1}; T(s)::Cre* embryo caudal ends ($p \leq 0.05$).

Stage Phenotype	E8.5	E8.75	E9.0	Combined
	None	Mild	Strong	
# of genes bound by SRF/total dysregulated genes (%)				
Downregulated genes	6/7 (85.7%)	10/26 (38.5%)	15/216 (6.9%)	19/230 (8.3%)
Upregulated genes	0/3 (0.0%)	3/113 (2.7%)	4/223 (1.8%)	6/316 (1.9%)
Total dysregulated genes	6/10 (60.0%)	13/139 (38.5%)	19/436 (6.9%)	25/546 (8.3%)

(Sun et al., 2006), hence, we restricted our analysis to these genomic distances. Among the over 19,100 genes represented on the microarray we identified 658 genes (p -value $\leq 1 \times 10^{-5}$) containing one or more SRF peaks within 4000 bp of the TSS. Among these 658 genes, only 18 genes were differentially expressed between *Srf^{flex1/flex1}; T(s)::Cre* embryos and heterozygous control embryos at all stages examined. Of those 18 genes, 12 (including *Srf*) have previously been described as SRF target genes, and six are novel putative *Srf* targets (Fig. 3). In addition, we identified seven genes which showed

differential expression in the microarray analysis, and have previously been shown to be bound by SRF in other cell types, but were not found to be bound by SRF in P19 cells. Taken together, we identified 25 genes that are bound by SRF and are dysregulated in the caudal ends of *Srf^{flex1/flex1}; T(s)::Cre* embryos. Of these 25 direct SRF target genes we found 19 to be downregulated in the absence of *Srf*, whereas only six were found to be upregulated. This is consistent with previous reports suggesting that SRF mainly acts as a transcriptional activator (Schlesinger et al., 2011).

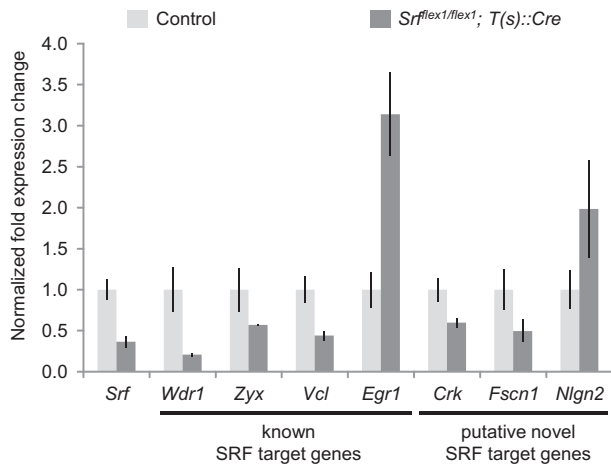


Fig. 4 – Validation of dysregulation of SRF target genes in *Srf^{flex1/flex1}; T(s)::Cre* caudal ends. Quantitative real-time PCR analysis of a subset of SRF target genes. Expression levels were analyzed in E8.75–E9.0 caudal ends of *Srf^{flex1/flex1}; T(s)::Cre* compared to *Srf^{flex1/+}; T(s)::Cre* embryos (control) (s.d., $n = 3$, $p \leq 0.05$) and normalized to the housekeeping genes *Gapdh* and *Hmbh*.

We validated the microarray data using qRT-PCR analysis on a subset of the SRF targets acting during axis elongation (Fig. 4). The qRT-PCR data confirmed the microarray data, suggesting that all 25 genes identified in this work are dependent on *Srf* during the process of axis elongation.

While the overall number of genes directly regulated by SRF increased over the three stages analyzed (E8.5 = 6, E8.75 = 13 and E9.0 = 19) their percentage with respect to the total number of dysregulated genes decreased (E8.5 = 60%, E8.75 = 9.4% and E9.0 = 4.3%) (Table 1). It is likely that the increase in dysregulated genes is due to altered tissue composition of later stage *Srf*-deficient embryos, rather than reflecting an increase in the number of SRF target genes at later stages. Hence, the SRF targets found here are those most likely to be causal for the axis elongation defect observed in *Srf*-deficient embryos.

2.4. SRF controls cell migration during axis elongation

In order to elucidate the primary function of the 25 direct SRF targets identified in the process of axis extension, we performed Gene Ontology analysis (Ingenuity® Pathway Analysis

Tool) (Table 2). The majority of these SRF target genes are found to be associated with cellular movement and cell morphology. Other functions identified were cellular assembly and organization, and cellular function and maintenance. Previous work in other systems showed that *Srf* is able to regulate cell motility and related functions (reviewed in Olson and Nordheim, 2010). Hence, the primary role of SRF in the process of axis elongation seems to be controlling genes involved in cell morphology and cellular movement.

To examine impaired cell morphology and migration in *Srf^{flex1/flex1}; T(s)::Cre* embryonic caudal ends, we analyzed caudal explants in an *ex vivo* system. Cell adhesion and migration of newly formed mesodermal cells emerging from the ps requires the extracellular matrix protein Fibronectin (George et al., 1997, 1993; Georges-Labouesse et al., 1996) and SRF-deficient embryonic stem cells are capable of attaching to Fibronectin-coated surfaces (Schrott et al., 2002). Using this knowledge we performed explant culture assays on Fibronectin-coated dishes to determine the migratory potential of SRF-deficient mesoderm (Fig. 5A). Caudal explants from both mutant and control embryos attached within one hour and cells began to migrate away from the explant. After 48 h of culture we measured the maximal distance between the explant and the edge of the migrating cells and observed a significant difference between SRF-deficient and control embryos (Fig. 5B). The maximum distance observed was $604 \mu\text{m} \pm 71 \mu\text{m}$ in mutant and $955 \mu\text{m} \pm 59 \mu\text{m}$ in control explants ($n = 5$) (student's t-test: $p = 2.9 \times 10^{-5}$). Explants migrate away after 5 h (300 min), while the cells from SRF deficient explants remain in close proximity to the explant tissue (Movie S1). As was seen in whole embryos, the number of apoptotic cells was increased in mesenchymal cells around the explants from the SRF mutants, while the number of mitotic cells did not change (Fig. 5C and D). However, the majority of cells that do not undergo apoptosis remain in close proximity to the explant, exhibiting a reduced migration capability (Movie S1). From these experiments we concluded that SRF is required *in vivo* to control the cellular capacity for migration during axis elongation.

2.5. The formation of stress fibers and focal adhesions is impaired in *Srf*-deficient embryo explants

In addition to impaired migration, we also observed that caudal cells derived from SRF-deficient embryo explants displayed differences in cell morphology as compared to

Table 2 – Main cellular functions of genes regulated by *Srf* during axial elongation, by GO analysis.

Category	p-Value range	# Of genes	Gene identities
Cellular movement	7.16×10^{-8} – 4.84×10^{-2}	16	<i>Actb, Anxa2, Anxa3, Cnn2, Crk, Dstn, Egr1, Fhl1, Fhl2, Fscn1, Pfn1, Srf, Tpm1, Tpm3, Vcl, Zyx</i>
Cell Morphology	2.43×10^{-7} – 4.45×10^{-2}	12	<i>Actb, Anxa2, Cnn2, Crk, Dstn, Egr1, Pfn1, Srf, Tpm1, Tpm3, Vcl, Zyx</i>
Cellular assembly and organization	2.12×10^{-6} – 4.86×10^{-2}	16	<i>Actb, Anxa2, Cnn2, Crk, Dstn, Fhl1, Fhl2, Fscn1, Nlgn2, Pdilm7, Pfn1, Srf, Tpm1, Tpm3, Vcl, Zyx</i>
Cellular function and maintenance	7.56×10^{-6} – 4.86×10^{-2}	18	<i>Actb, Anxa2, Anxa3, Cnn2, Crk, Dstn, Egr1, Fhl1, Fhl2, Fscn1, Nlgn2, Pdilm7, Pfn1, Srf, Tpm1, Tpm3, Vcl, Zyx</i>
Cell cycle	5.07×10^{-4} – 4.05×10^{-2}	4	<i>Dstn, Egr1, Pfn1, Tpm1</i>

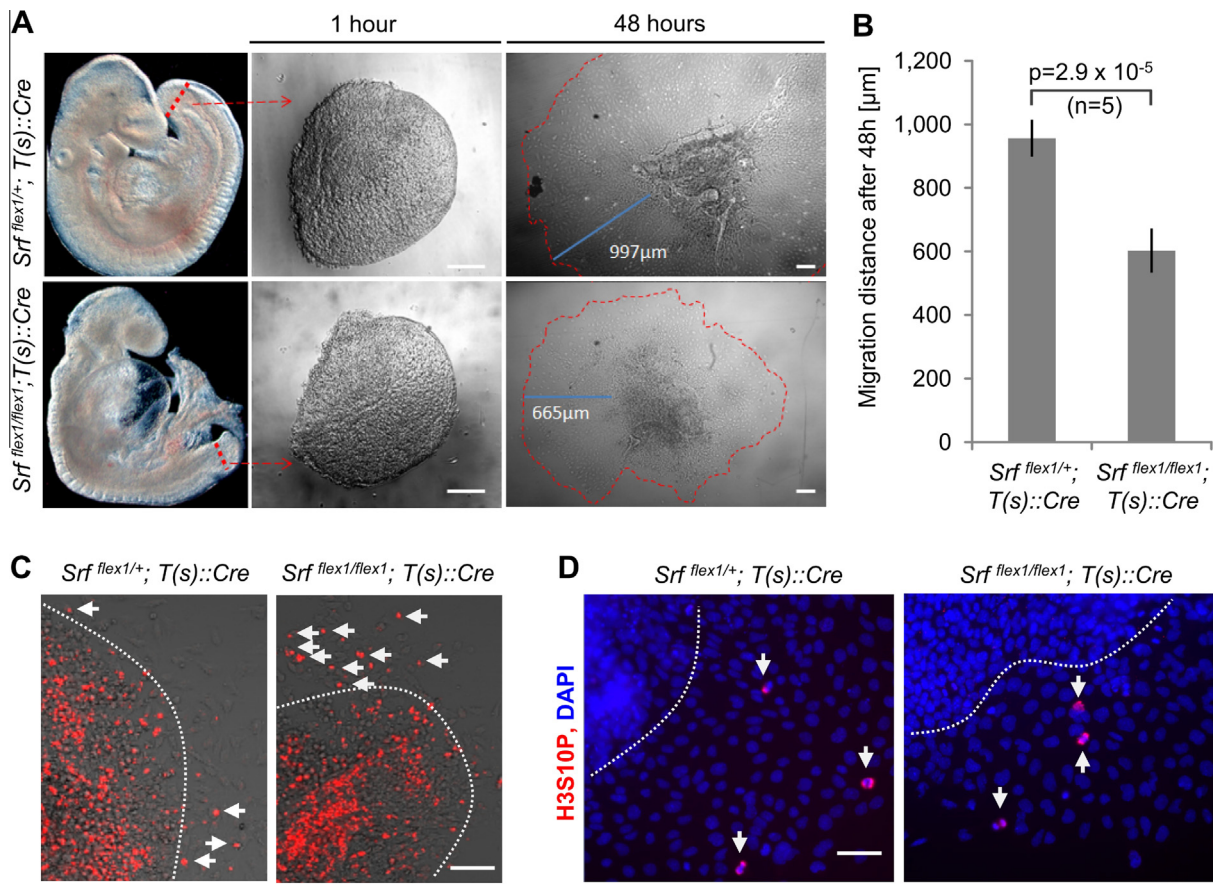


Fig. 5 – SRF-deficiency results in impaired migration of mesodermal cells *ex vivo*. (A) Caudal ends were dissected from *Srf^{flex1/flex1}; T(s)::Cre* and *Srf^{flex1/+}; T(s)::Cre* (control) embryos (representative embryos, level indicated by the dashed red lines), divided along the midline, and plated with the medial surface facing down onto Fibronectin-coated dishes. After one hour the explants adhered to the surface and cells began to spread. After two days, the maximum distance from the original explant was measured (shown by the blue line). Scale bars (white) represent 150 µm. (B) Maximal distance between the border of the occupied area and the original explant (n = 5) from *Srf^{flex1/+}; T(s)::Cre* and *Srf^{flex1/flex1}; T(s)::Cre* explants after 48 h. The s.d. is given. (C) Representative LysoTracker® Red staining of explants to visualize apoptotic cells. The white arrows point to apoptotic cells. Scale bar represents 50 µm. (D) Representative H3S10P staining of explants to visualize proliferating cells. The white arrows point to mitotic nuclei. Scale bar represents 50 µm.

control embryos. While most of the cells from control samples were long and spindle-shaped, typical hallmarks of motile mesenchymal cells, the cells from SRF-deficient caudal ends appeared small and rounded (Fig. 6A). Several of the genes that we identified to be regulated by SRF in embryonic caudal ends encode actin monomers (*Actb*, *Acta2*), proteins involved in cytoskeletal actin organization (*Tpm1*, *Tpm3*, *Tpm4*, *Wdr1*, *Pdim7*, *Cnn2*, *Dstn*, *Anxa2*, *Fscn1*) or in the formation of focal adhesions (*Zyx*, *Vcl*, *Fhl2*, *Crk*). We reasoned that the altered cell morphology observed in SRF-deficient explants might be due to defective formation of actin stress fibers and focal adhesions. To examine this possibility we stained control and mutant explants with FITC conjugated Phalloidin, to visualize F-actin fibers. The staining revealed reduced F-actin level in cells originating from SRF-deficient caudal ends as compared to controls (Fig. 6B), in agreement with the observed decrease in expression of genes encoding actin (Table 2). Furthermore, we noted a drastic difference in the structure of the cytoskeleton. While cells from control samples displayed stress fibers which traversed the entire cell

body, these structures were significantly reduced in cells from SRF-deficient explants (Fig. 6B). Immunofluorescent staining using an antibody against the focal adhesion protein Vinculin further showed impaired focal adhesion formation in SRF-deficient cells (Fig. 6C). These cells displayed a mesenchymal character, as they were positive for Vimentin and no membrane associated E-cadherin was detected (Fig. 6C). Since stress fibers and focal adhesions are essential cytoskeletal elements for migratory cells, their absence provides a molecular explanation for the observed impairment of cell migration in SRF-deficient embryo explants.

3. Discussion

SRF has previously been shown to be essential for neuronal migration in the mouse forebrain (Alberti et al., 2005), as well as for spreading, adhesion, and migration of murine ES cells (Schratt et al., 2002). In both of these prior studies down-regulation of genes encoding either actin monomers (*Actb*) or proteins required for focal adhesion formation (*Zyx*, *Vcl*)

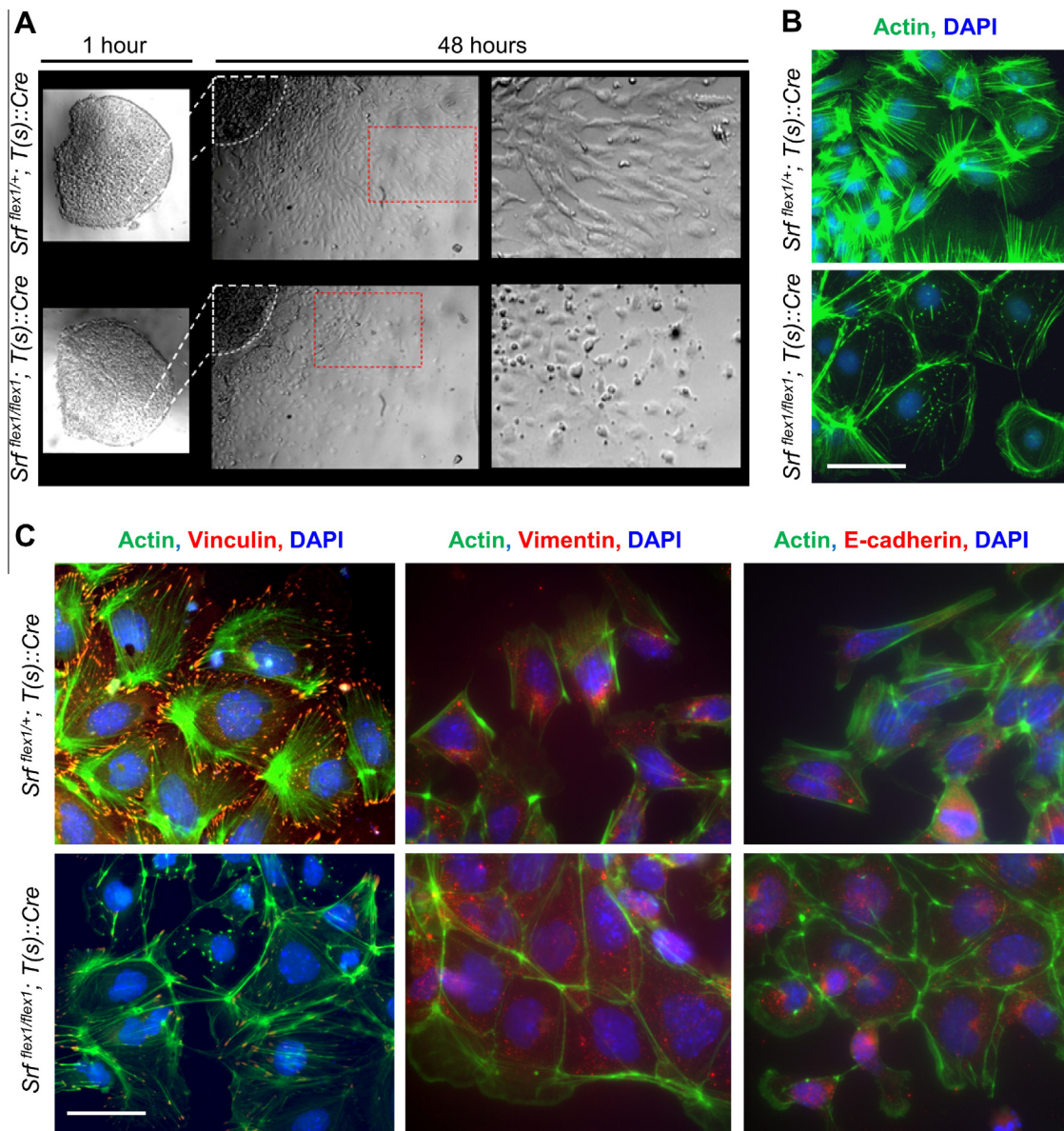


Fig. 6 – SRF-deficiency in mesodermal cells affects cell morphology and cytoskeletal arrangement. (A) Representative images from caudal end explants from *ex vivo* migration assays. Images on the right show magnifications of the boxed areas in the middle panels. **(B)** Representative fluorescence images from cells at the border of the explant culture after 48 h with Actin visualized in the migratory cells using phalloidin (green) and nuclei with DAPI (blue). Scale bar represents 50 μm . **(C)** Immunofluorescent staining of focal adhesions (Vinculin, red) and markers of mesenchymal cells (Vimentin, non-membrane bound E-cadherin, red). Counterstaining was performed for Actin (phalloidin, green) and nuclei (DAPI, blue). Scale bar represents 50 μm .

caused impaired cell motility in *Srf* mutants associated with defective formation of actin stress fibers and focal adhesion plaques. Here we show that SRF is also essential for proper migration of nascent mesoderm formed at the ps of mid-gestation mouse embryos. We provide evidence that SRF is required for reorganization of the actin cytoskeleton in nascent mesoderm, and identify it as a crucial factor for A–P axis elongation.

In searching for direct SRF target genes acting in axis development on a genome-wide level, we identified several novel SRF targets, along with a number of previously

described targets (Fig. 3). Of note, v-crk sarcoma virus CT10 oncogene homolog (avian) (*Crk1*) and Fascin homolog 1 actin bundling protein (*Fscn1*) encode proteins associated with cell morphology and cellular motility. *Fscn1* is widely expressed throughout the embryo including in developing somites (De Arcangelis et al., 2004), and has been implicated in tumor cell migration and invasiveness (Grothey et al., 2000a, 2000b). Inhibition of the Fascin–Actin interaction in C2C12 myoblast cells interferes with cell migration and cytoskeletal organization (Adams and Schwartz, 2000). Similarly, *Crk* encodes a protein involved in focal adhesion formation and

in remodeling of the cytoskeleton at focal adhesions (Feller, 2001). Knockdown of *Crk* in NIH-3T3 fibroblasts resulted in decreased PDGF-stimulated migratory ability (Antoku and Mayer, 2009). These findings, together with our data, suggest that downregulation of *Fscn1* and/or *Crk1* in SRF-deficient mid-gestation embryos may significantly contribute to the altered morphology and impaired migratory ability of mesodermal cells in these mutants.

Most of the genes we identified as direct SRF targets in the ps-derived nascent mesoderm are related to cytoskeletal actin reorganization and it was previously shown that genes like *Vcl*, *Cnn2*, and others are regulated by SRF in combination with the myocardin-related transcription factors MRTF-A and MRTF-B (Olson and Nordheim, 2010). The activity of MRTF cofactors, in turn, is controlled by Rho-dependent actin turnover (Miralles et al., 2003). In the ps of mid-gestational mouse embryos, the disruption of E-cadherin-mediated epithelial cell–cell contacts is indispensable for the ability of cells to undergo EMT and gain motility. Previous reports have demonstrated that the degradation of E-cadherin directly regulates SRF–MRTF activity via the Rho family member RAC1 (Busche et al., 2008). It is likely that the initial steps in cytoskeletal reorganization required for mesoderm formation during axis elongation utilize SRF in a complex with MRTF cofactors in order to execute the complete program for adopting a migratory capability.

A correlation between impaired mesodermal cell migration and arrested axis elongation has previously been shown in several models. For example, treatment of chick embryos with the cell motility inhibitors Y27632 and blebbistatin causes delayed axis elongation (Bénazéraf et al., 2010). In migrating cells, the focal adhesion complexes are attached to the ECM, and this attachment requires integrins. There are several studies in mouse embryos showing that interfering with proper expression of either the ECM protein coding gene *Fibronectin* or members of the *Integrin* family can cause axis truncations (George et al., 1993; Georges-Labouesse et al., 1996; Yang et al., 1999). In order to migrate, cells generate a force against the ECM by contracting actin stress fibers that are attached to the focal adhesions (McHardy et al., 2005). Consequently, impaired function of either *Fibronectin* or members of the *Integrin* family affects mesodermal cell migration. In fact, a mutation in the RGD motif of *Fibronectin* ($Fn^{RGE/RGE}$) results in impaired axis elongation, which becomes apparent at E9.0 due to a shift in integrin usage by mesodermal cells at this stage (Girós et al., 2011). Interestingly, the phenotype of $Fn^{RGE/RGE}$ embryos closely resembles the phenotype of $Srf^{flex1/flex1}; T(s)::Cre$ embryos since, in addition to axis truncation at E8.75–E9.0, both mutants have heart malformations. This suggests that the heart phenotype of $Srf^{flex1/flex1}; T(s)::Cre$ embryos may also be partly a result of impaired cell migration and not solely due to the role of SRF in heart differentiation.

The gene *Egr1*, which is among the best studied SRF targets, was found to be upregulated upon loss of SRF in the caudal region of $Srf^{flex1/flex1}; T(s)::Cre$ embryos, suggesting that *Egr1* is repressed by SRF in this context. Similar observations were reported by Sullivan and coworkers using a conditional knock-out of *Srf* in macrophages (Sullivan et al., 2011). *Egr1* is known to be involved in cellular growth control and can

control proliferation in hematopoietic stem cells (Min et al., 2008). Thus, the downregulation of genes involved in cytoskeletal reorganization into a mesenchymal, motile cell type upon loss of *Srf*, and the simultaneous upregulation of *Egr1*, might suggest that cell differentiation and cell proliferation also have to be precisely balanced during axis elongation.

It is noteworthy that, since we used *T* driven expression of *Cre* to inactivate *Srf*, *Srf* should be inactivated in nascent mesoderm beginning with primitive streak formation at around E6.5 however, axis elongation was not visibly affected until E9.0, similar to embryos homozygous for *T/T* (Yanagisawa et al., 1981). This indicates a similar change in requirement for *Srf* and *T* in early mesoderm formation, as opposed to mesoderm formation at mid-gestation. Several reports have indicated that the latter function of *T* comprises the maintenance of axial stem cells, though there is not yet direct proof for this proposition (for review see Kondoh and Takemoto, 2012). Analogous to *T*, *Srf* might have an indirect role in the maintenance of axial stem cells by regulating migratory potential. In support of this hypothesis, it has been suggested that loss of *B1 Sox* gene expression in multipotential paraxial precursor cells causes increased migration into the mesodermal compartment and, thereby, increased production of mesodermal tissue (Yoshida et al., 2014). Thus, one might argue that the production of mesodermal tissue decreases when migration is impaired; consequently causing axis extension to arrest.

In summary, we show here that during axis elongation a small subset of genes directly depend on SRF and these genes associate primarily with migratory functions in nascent mesodermal cells. This further highlights that, after the initiation of EMT in which E-cadherin is degraded, nascent mesodermal cells have to adopt migratory capabilities in order to properly form the A–P body axis.

4. Materials and methods

4.1. In situ hybridization

Whole mount *in situ* hybridization was carried out using the standard protocol described on the MAMEP website (<http://mamep.molgen.mpg.de>). The *Srf* probe was generated by PCR on cDNA from whole embryos (E9.5) and subcloned into pBluescript II SK(+) (Stratagene) and covers the complete coding region of *Srf*.

4.2. Analysis of gene expression

Quantitative real-time PCR (qPCR): Total RNA was isolated from embryos using the RNeasyMini Kit (Qiagen). Reverse transcription of RNA into cDNA was performed using the SuperScript II First-Strand Synthesis System (Invitrogen). All procedures were performed according to the manufacturer's instructions. Gene expression was analyzed by qPCR using Power SYBR Green PCR Master Mix (Applied Biosystems). The reactions were run in triplicate on a StepOnePlus Real-Time PCR System, and the results were analyzed using the StepOnePlus Software v2.0.2 (Applied Biosystems).

For amplification of transcripts, primers with the following sequences were used: *Gapdh_fwd*: TGAGAGAGGCCAGCTAC TC, *Gapdh_rev*: AGGGCTGCAGTCCGTATTTA; *Hbms_fwd*: CCT GGGCGGAGTCATGTC, *Hbms_rev*: ACTCGAATCACCTCATCTT TGA; *Srf_fwd*: AGGGCTGCAGTCCGTATTTA, *Srf_rev*: AGGTATC CCCCAACCTTC; *Wdr1_fwd*: GGTCGCGTCAGTCACTT, *Wdr1_rev*: CCCCAGCTTTGACCATA; *Vcl_fwd*: ATCAATCCCTG GCTTCACAC, *Vcl_rev*: TTTCAAAGT GCCCATGACAA; *Zyx_fwd*: CAGTGCTTACCTGTGTGGT, *Zyx_rev*: CCTTGGAGCGTATTGCT TGT; *Egr1_fwd*: GGCCGGTCTTCCATATT, *Egr1_rev*: CGAATCG GCCTCTATTCAA, *Crk_fwd*: CAGCTCTCCGTGAAGCCTAC, *Crk_rev*: AGCCAAATCCAACCAACAG; *Fscn1_fwd*: AGATGCTT GGCTCCTGTCC, *Fscn1_rev*: GAGGTGTCTGGGAAGACGTG; *Nlgn2_fwd*: CCTGAGCCCTGTAAGCAGAT, *Nlgn2_rev*: ATTGGAG TCCGTGGCTGTAT.

Gene expression profiles of *Srf^{fl^{ex1}/fl^{ex1}}; T(s)::Cre* caudal ends at E8.5, 8.75 and 9.0 and those of the appropriate heterozygous littermates were analyzed using Illumina whole-genome expression arrays (Illumina Mouse Ref-8 v2.0). For each sample, four biological replicates were compared to four control samples. RNA was isolated from embryonic caudal ends using the RNeasy Mini Kit (Qiagen), and labeled using the Illumina TotalPrep RNA Amplification Kit (Ambion). All procedures were performed according to the manufacturer's instructions. 1 μ g of cRNA was hybridized to MouseRef-8 v2.0 Expression BeadChip (Illumina). Arrays were scanned on the Illumina BeadArray Reader and expression data were processed using the lumiR/Bioconductor package (Du et al., 2008). Raw data were analyzed using background subtraction (bgAdjust) and the quantile normalization method. Differentially expressed genes were identified using the limma1 package. Genes were considered to be significantly dysregulated when they had a fold change $\geq \log_2^{0.4}$, $p \leq 0.05$.

The GEO accession number for the expression data in this paper is GSE44406.

4.3. Chromatin immunoprecipitation and massive parallel sequencing

For the SRF-ChIP we used a P19 cell line stably transfected with a plasmid containing a neomycin resistance gene and a CAGGS promoter-driven *Srf* transgene, coding for a SRF containing an Avi-tag (SLNDIFEAQKIEW) at the C-terminus. The cells were cultivated under standard conditions. At a confluence of 70–80% (approx. $2.5\text{--}4 \times 10^7$ cells on a 10 cm dish), the cells were cross-linked with 0.75% formaldehyde for 10 min at room temperature, followed by a 5 min incubation with glycine (0.125 M). Cells were scraped from the dish, washed three times with PBS and lysed using 400 μ l Upstate lysis buffer at 7 $^{\circ}$ C for 30 min in a thermoshaker at 750 rpm. Chromatin was fragmented with a Branson Digital Sonifier II W-450 (3 mm tip) using 6×10 s pulses with 50 s breaks and fragmentation was verified on an agarose gel (mean size ~ 300 bp). The sample was centrifuged (10,000 rcf, 1 min, 8 $^{\circ}$ C) and used for ChIP according to the Upstate protocol, using 2 μ g of SRF antibody (Santa Cruz; sc-335 X) in a 400 μ l total volume. To decrease nonspecific binding of DNA, the washing times were increased from 8 min to 16 min. Massive parallel

sequencing was performed by single read analysis with the Illumina Genome Analyzer. Library preparation and sequencing was performed by the Next Generation Sequencing Core Facility at Max-Planck Institute for Molecular Genetics according to the Illumina ChIP-seq standard protocol. Sequences were mapped against the mouse genome using the bowtie software (Langmead et al., 2009) and peaks were identified with SICER (Zang et al., 2009).

4.4. Ex vivo migration assay

To analyze the migratory potential of SRF-deficient mesodermal cells, caudal ends from E9.5 *Srf^{fl^{ex1}/fl^{ex1}}; T(s)::Cre* and from control littermate embryos were dissected, split along the midline and plated on μ -slides (ibidi; Martinsried). The slides had been coated one day earlier with the extracellular matrix protein Fibronectin (Calbiochem #341631). For this purpose, Fibronectin was diluted (1:100) with PBS, pipetted onto the μ -slides, and stored at 4 $^{\circ}$ C. Shortly before usage, the Fibronectin was washed off twice with PBS, and DMEM/10% FBS was added. The embryonic tissue was placed cut side down onto slides and attached within one hour. Next, medium was removed until the tissue was at the air/liquid interface and the explants were cultivated under standard cell culture conditions. Medium was exchanged daily. After two days, the maximal migration distance was measured and explants were processed for immunofluorescence.

For the timelapse analysis the explants were analyzed on a Zeiss LSM710NLO in an incubation chamber under 65% O₂, 5% CO₂ and 30% N₂ conditions in DMEM F12 media containing 5 mM Glucose, 1 mM Glutamine and 1% BSA (Lauschke et al., 2013). A z-stack of 5 images with 2×2 overlapping tiles was taken every 20 min using the ZEN software (Zeiss). Single projected and stitched images were then used to compile the movie using the ImageJ software.

4.5. Immunohistochemistry

Whole embryos were fixed in 4% paraformaldehyde overnight. Following standard ethanol processing they were embedded in paraffin and sectioned at 5 μ m. Sections were incubated with anti-Brachyury (1:400, R&D Systems), anti-E-cadherin (1:200, BD Bioscience), anti-Vimentin (1:50, Santa Cruz) and anti-H3S10P (1:500, Millipore) primary antibodies. After counterstaining with secondary Cy3 coupled antibodies (Life Technologies), sections were mounted using VECTA-SHIELD mounting medium with DAPI (Vector Laboratories Inc.).

Explants from the *ex vivo* assay were stained using Phalloidin-Fluorescein-isothiocyanate (FITC) conjugate (Sigma) according to the manufacturer's instructions at a dilution of 1:50 in PBS. Primary antibodies were used as described above and focal adhesions were visualized using an antibody against Vinculin (Abcam), according to standard procedures at a dilution of 1:100.

For visualization of apoptotic cells, LysoTracker[®] Red DND-99 (Life Technologies) was used on the explants as described previously (Zucker et al., 1999).

4.6. Flow cytometry analysis of apoptotic cells

Embryo cell suspensions were prepared by incubating head or tail fractions, or single explants in 0.05% Trypsin/EDTA for 5 min on ice with occasional shaking. Trypsin was quenched by adding 5% BSA/PBS for 5 min and the single suspension washed twice with PBS on ice. The Annexin-V-FLUOS (Roche) staining kit was used according to the manufacturer's protocol. Prior to analysis on a FACS Aria II (BD Biosciences) the suspension was filtered through a 30 μ m mesh filter (BD Biosciences). The data were analyzed using the FlowJo software (Treestar).

Acknowledgments

We thank Achim Gossler for providing the T(s)::Cre mouse strain. Thanks also to Manuela Scholze for help with embryo isolation and Tracie Pennimpede for comments on the manuscript. A.N. received funding by the DFG (Grant No. 120/12-4).

Appendix A. Supplementary data

Supplementary data associated with this article can be found, in the online version, at <http://dx.doi.org/10.1016/j.mod.2014.07.001>.

REFERENCES

- Adams, J.C., Schwartz, M.A., 2000. Stimulation of fascin spikes by thrombospondin-1 is mediated by the GTPases Rac and Cdc42. *J. Cell Biol.* 150, 807–822.
- Alberti, S., Krause, S.M., Kretz, O., Philippar, U., Lemberger, T., Casanova, E., Wiebel, F.F., Schwarz, H., Frotscher, M., Schütz, G., Nordheim, A., 2005. Neuronal migration in the murine rostral migratory stream requires serum response factor. *Proc. Natl. Acad. Sci. USA* 102, 6148–6153.
- Antoku, S., Mayer, B.J., 2009. Distinct roles for Crk adaptor isoforms in actin reorganization induced by extracellular signals. *J. Cell Sci.* 122, 4228–4238.
- Arsenian, S., Weinhold, B., Oelgeschläger, M., Rütter, U., Nordheim, A., 1998. Serum response factor is essential for mesoderm formation during mouse embryogenesis. *EMBO J.* 17, 6289–6299.
- Barron, M.R., Belaguli, N.S., Zhang, S.X., Trinh, M., Iyer, D., Merlo, X., Lough, J.W., Parmacek, M.S., Bruneau, B.G., Schwartz, R.J., 2005. Serum response factor, an enriched cardiac mesoderm obligatory factor, is a downstream gene target for Tbx genes. *J. Biol. Chem.* 280, 11816–11828.
- Baum, B., Settleman, J., Quinlan, M.P., 2008. Transitions between epithelial and mesenchymal states in development and disease. *Semin. Cell Dev. Biol.* 19, 294–308.
- Beddington, R.S., 1983. Histogenetic and neoplastic potential of different regions of the mouse embryonic egg cylinder. *J. Embryol. Exp. Morphol.* 75, 189–204.
- Bénazéraf, B., Francois, P., Baker, R.E., Denans, N., Little, C.D., Pourquie, O., 2010. A random cell motility gradient downstream of FGF controls elongation of an amniote embryo. *Nature* 466, 248–252.
- Ben-Haim, N., Lu, C., Guzman-Ayala, M., Pescatore, L., Mesnard, D., Bischofberger, G., Naef, F., Robertson, E.J., Constam, D.B., 2006. The nodal precursor acting via activin receptors induces mesoderm by maintaining a source of its convertases and BMP4. *Dev. Cell* 11, 313–323.
- Busche, S., Descot, A., Julien, S., Genth, H., Posern, G., 2008. Epithelial cell–cell contacts regulate SRF-mediated transcription via Rac-actin-MAL signalling. *J. Cell Sci.* 121, 1025–1035.
- Catala, F., Wanner, R., Barton, P., Cohen, A., Wright, W., Buckingham, M., 1995. A skeletal muscle-specific enhancer regulated by factors binding to E and CARG boxes is present in the promoter of the mouse myosin light-chain 1A gene. *Mol. Cell Biol.* 15, 4585–4596.
- Ciruna, B., Rossant, J., 2001. FGF signaling regulates mesoderm cell fate specification and morphogenetic movement at the primitive streak. *Dev. Cell* 1, 37–49.
- Croissant, J.D., Kim, J.H., Eichele, G., Goering, L., Lough, J., Prywes, R., Schwartz, R.J., 1996. Avian serum response factor expression restricted primarily to muscle cell lineages is required for alpha-actin gene transcription. *Dev. Biol.* 177, 250–264.
- Cunningham, T.J., Zhao, X., Duester, G., 2011. Uncoupling of retinoic acid signaling from tailbud development before termination of body axis extension. *Genesis* 49, 776–783.
- De Arcangelis, A., Georges-Labouesse, E., Adams, J.C., 2004. Expression of fascin-1, the gene encoding the actin-bundling protein fascin-1, during mouse embryogenesis. *Gene Exp. Pat.* 4, 637–643.
- Du, P., Kibbe, W.A., Lin, S.M., 2008. Lumi: a pipeline for processing Illumina microarray. *Bioinformatics* 24, 1547–1548.
- Feller, S.M., 2001. Crk family adaptors-signalling complex formation and biological roles. *Oncogene* 20, 6348–6371.
- Feller, J., Schneider, A., Schuster-Gossler, K., Gossler, A., 2008. Noncyclic Notch activity in the presomitic mesoderm demonstrates uncoupling of somite compartmentalization and boundary formation. *Genes Dev.* 22, 2166–2171.
- George, E.L., Georges-Labouesse, E.N., Patel-King, R.S., Rayburn, H., Hynes, R.O., 1993. Defects in mesoderm, neural tube and vascular development in mouse embryos lacking fibronectin. *Development* 119, 1079–1091.
- George, E.L., Baldwin, H.S., Hynes, R.O., 1997. Fibronectins are essential for heart and blood vessel morphogenesis but are dispensable for initial specification of precursor cells. *Blood* 90, 3073–3081.
- Georges-Labouesse, E.N., George, E.L., Rayburn, H., Hynes, R.O., 1996. Mesodermal development in mouse embryos mutant for fibronectin. *Dev. Dyn.* 207, 145–156.
- Girós, A., Grgur, K., Gossler, A., Costell, M., 2011. α 5 β 1 integrin-mediated adhesion to fibronectin is required for axis elongation and somitogenesis in mice. *PLoS One* 6, e22002.
- Grothey, A., Hashizume, R., Ji, H., Tubb, B.E., Patrick, C.W., Yu, D., Mooney, E.E., McCrea, P.D., 2000a. C-erbB-2/HER-2 upregulates fascin, an actin-bundling protein associated with cell motility, in human breast cancer cell lines. *Oncogene* 19, 4864–4875.
- Grothey, A., Hashizume, R., Sahin, A.A., McCrea, P.D., 2000b. Fascin, an actin-bundling protein associated with cell motility, is upregulated in hormone receptor negative breast cancer. *Br. J. Cancer* 83, 870–873.
- Herrmann, B.G., 1991. Expression pattern of the Brachyury gene in whole-mount TWis/TWis mutant embryos. *Development* 117, 913–917.
- Johansen, F.E., Prywes, R., 1995. Serum response factor: transcriptional regulation of genes induced by growth factors and differentiation. *Biochim. Biophys. Acta* 1242, 1–10.
- Jung, C., Lim, J.H., Choi, Y., Kim, D., Kang, K.J., Noh, S.-M., Im, D.-S., 2010. Enigma negatively regulates p53 through MDM2 and promotes tumor cell survival in mice. *J. Clin. Invest.* 120, 4493–4506.
- Kemler, R., Hierholzer, A., Kanzler, B., Kuppig, S., Hansen, K., Taketo, M.M., de Vries, W.N., Knowles, B.B., Solter, D., 2004.

- Stabilization of beta-catenin in the mouse zygote leads to premature epithelial–mesenchymal transition in the epiblast. *Development* 131, 5817–5824.
- Kondoh, H., Takemoto, T., 2012. Axial stem cells deriving both posterior neural and mesodermal tissues during gastrulation. *Curr. Opin. Genet. Dev.* 22, 374–380.
- Langmead, B., Trapnell, C., Pop, M., Salzberg, S.L., 2009. Ultrafast and memory-efficient alignment of short DNA sequences to the human genome. *Genome Biol.* 10, R25.
- Lauschke, V.M., Tsiairis, C.D., François, P., Aulehla, A., 2013. Scaling of embryonic patterning based on phase-gradient encoding. *Nature* 493, 101–105.
- Levayer, R., Lecuit, T., 2008. Breaking down EMT. *Nat. Cell Biol.* 10, 757–759.
- Lim, J., Thiery, J.P., 2012. Epithelial–mesenchymal transitions: insights from development. *Development* 139, 3471–3486.
- Luxenburg, C., Pasolli, H.A., Williams, S.E., Fuchs, E., 2011. Developmental roles for Srf, cortical cytoskeleton and cell shape in epidermal spindle orientation. *Nat. Cell Biol.* 13, 203–214.
- Martin, B.L., Kimelman, D., 2012. Canonical Wnt signaling dynamically controls multiple stem cell fate decisions during vertebrate body formation. *Dev. Cell* 22, 223–232.
- McBurney, M.W., 1993. P19 embryonal carcinoma cells. *Int. J. Dev. Biol.* 37, 135–140.
- McHardy, L.M., Warabi, K., Andersen, R.J., Roskelley, C.D., Roberge, M., 2005. Strongylophorine-26, a Rho-dependent inhibitor of tumor cell invasion that reduces actin stress fibers and induces nonpolarized lamellipodial extensions. *Mol. Cancer Ther.* 4, 772–778.
- Miano, J.M., 2003. Serum response factor: toggling between disparate programs of gene expression. *J. Mol. Cell. Cardiol.* 35, 577–593.
- Miano, J.M., 2008. Deck of CARGs. *Circ. Res.* 103, 13–15.
- Min, I.M., Pietramaggiore, G., Kim, F.S., Passequé, E., Stevenson, K.E., Wagers, A.J., 2008. The transcription factor EGR1 controls both the proliferation and localization of hematopoietic stem cells. *Cell Stem Cell* 2, 380–391.
- Miralles, F., Posern, G., Zaromytidou, A., Treisman, R., 2003. Actin dynamics control SRF activity by regulation of its coactivator MAL. *Cell* 113, 329–342.
- Mohun, T.J., Chambers, A.E., Towers, N., Taylor, M.V., 1991. Expression of genes encoding the transcription factor SRF during early development of *Xenopus laevis*: identification of a CARG box-binding activity as SRF. *EMBO J.* 10, 933–940.
- Moiseyeva, E.P., Weller, P.A., Zhidkova, N.I., Corben, E.B., Patel, B., Jasinska, I., Koteliensky, V.E., Critchley, D.R., 1993. Organization of the human gene encoding the cytoskeletal protein vinculin and the sequence of the vinculin promoter. *J. Biol. Chem.* 268, 4318–4325.
- Nakaya, Y., Sheng, G., 2008. Epithelial to mesenchymal transition during gastrulation: an embryological view. *Dev. Growth Differ.* 50, 755–766.
- Norman, C., Runswick, M., Pollock, R., Treisman, R., 1988. Isolation and properties of cDNA clones encoding SRF, a transcription factor that binds to the c-fos serum response element. *Cell* 55, 989–1003.
- Olson, E.N., Nordheim, A., 2010. Linking actin dynamics and gene transcription to drive cellular motile functions. *Nat. Rev. Mol. Cell Biol.* 11, 353–365.
- O’Sullivan, N.C., Pickering, M., Di Giacomo, D., Loscher, J.S., Murphy, K.J., 2010. Mkl transcription cofactors regulate structural plasticity in hippocampal neurons. *Cereb. Cortex* 20, 1915–1925.
- Parlakian, A., Tuil, D., Hamard, G., Tavernier, G., Hentzen, D., Concordet, J.-P., Paulin, D., Li, Z., Daegelen, D., 2004. Targeted inactivation of serum response factor in the developing heart results in myocardial defects and embryonic lethality. *Mol. Cell. Biol.* 24, 5281–5289.
- Philippart, U., Schratt, G., Dieterich, C., Müller, J.M., Galgóczy, P., Engel, F.B., Keating, M.T., Gertler, F., Schüle, R., Vingron, M., Nordheim, A., 2004. The SRF target gene Fhl2 antagonizes RhoA/MAL-dependent activation of SRF. *Mol. Cell* 16, 867–880.
- Schlesinger, J., Schueler, M., Grunert, M., Fischer, J.J., Zhang, Q., Krueger, T., Lange, M., Tönjes, M., Dunkel, I., Sperling, S.R., 2011. The cardiac transcription network modulated by Gata4, Mef2a, Nkx2.5, Srf, histone modifications, and microRNAs. *PLoS Genet.* 7, e1001313.
- Schratt, G., Philippart, U., Berger, J., Schwarz, H., Heidenreich, O., Nordheim, A., 2002. Serum response factor is crucial for actin cytoskeletal organization and focal adhesion assembly in embryonic stem cells. *J. Cell Biol.* 156, 737–750.
- Schratt, G., Philippart, U., Hockemeyer, D., Schwarz, H., Alberti, S., Nordheim, A., 2004. SRF regulates Bcl-2 expression and promotes cell survival during murine embryonic development. *EMBO J.* 23, 1834–1844.
- Selvaraj, A., Prywes, R., 2004. Expression profiling of serum inducible genes identifies a subset of SRF target genes that are MKL dependent. *BMC Mol. Biol.* 5, 13.
- Shore, P., Sharrocks, A.D., 1995. The MADS-box family of transcription factors. *Eur. J. Biochem.* 229, 1–13.
- Spencer, J.a., Misra, R.P., 1999. Expression of the SRF gene occurs through a Ras/Sp/SRF-mediated-mechanism in response to serum growth signals. *Oncogene* 18, 7319–7327.
- Sullivan, A.L., Benner, C., Heinz, S., Huang, W., Xie, L., Miano, J.M., Glass, C.K., 2011. Serum response factor utilizes distinct promoter- and enhancer-based mechanisms to regulate cytoskeletal gene expression in macrophages. *Mol. Cell. Biol.* 31, 861–875.
- Sun, Q., Chen, G., Streb, J.W., Long, X., Yang, Y., Stoeckert, C.J., Miano, J.M., 2006. Defining the mammalian CARGome. *Genome Res.* 16, 197–207.
- Takada, S., Stark, K.L., Shea, M.J., Vassileva, G., McMahon, J.A., McMahon, A.P., 1994. Wnt-3a regulates somite and tailbud formation in the mouse embryo. *Genes Dev.* 8, 174–189.
- Van der Heyden, M.A.G., Defize, L.H.K., 2003. Twenty one years of P19 cells: what an embryonal carcinoma cell line taught us about cardiomyocyte differentiation. *Cardiovasc. Res.* 58, 292–302.
- Watson, D.K., Robinson, L., Hodge, D.R., Kola, I., Papas, T.S., Seth, A., 1997. FLI1 and EWS-FLI1 function as ternary complex factors and ELK1 and SAP1a function as ternary and quaternary complex factors on the Egr1 promoter serum response elements. *Oncogene* 14, 213–221.
- Wieland, F.F., Rennekampff, V., Vinterstein, K., Nordheim, A., 2002. Generation of mice carrying conditional knockout alleles for the transcription factor SRF. *Nucleic Acids Res.* 30, 124–126.
- Wilkinson, D.G., Bhatt, S., Herrmann, B.G., 1990. Expression pattern of the mouse T gene and its role in mesoderm formation. *Nature* 343, 657–659.
- Wilson, V., Olivera-Martinez, I., Storey, K.G., 2009. Stem cells, signals and vertebrate body axis extension. *Development* 136, 1591–1604.
- Yanagisawa, K.O., Fujimoto, H., Urushihara, H., 1981. Effects of the brachyury (T) mutation on morphogenetic movement in the mouse embryo. *Dev. Biol.* 87, 242–248.
- Yang, J.T., Bader, B.L., Kreidberg, J.A., Ullman-Culleré, M., Trevithick, J.E., Hynes, R.O., 1999. Overlapping and independent functions of fibronectin receptor integrins in early mesodermal development. *Dev. Biol.* 215, 264–277.
- Yeom, Y.I., Fuhrmann, G., Ovitt, C.E., Brehm, A., Ohbo, K., Gross, M., Hübner, K., Schöler, H.R., 1996. Germline regulatory element of Oct-4 specific for the totipotent cycle of embryonal cells. *Development* 122, 881–894.

-
- Yoshida, M., Uchikawa, M., Rizzoti, K., Lovell-Badge, R., Takemoto, T., Kondoh, H., 2014. Regulation of mesodermal precursor production by low-level expression of B1 Sox genes in the caudal lateral epiblast. *Mech. Dev.* 132, 59–68.
- Zang, C., Schones, D.E., Zeng, C., Cui, K., Zhao, K., Peng, W., 2009. A clustering approach for identification of enriched domains from histone modification ChIP-Seq data. *Bioinformatics* 25, 1952–1958.
- Zohn, I.E., Li, Y., Skolnik, E.Y., Anderson, K.V., Han, J., Niswander, L., 2006. P38 and a p38-interacting protein are critical for downregulation of E-cadherin during mouse gastrulation. *Cell* 125, 957–969.
- Zucker, R.M., Hunter, E.S., Rogers, J.M., 1999. Apoptosis and morphology in mouse embryos by confocal laser scanning microscopy. *Methods* 18, 473–480.